arXiv:cond-mat/0112460v1 [cond-mat.stat-mech] 26 Dec 2001

Scaling of Cluster and Backbone Mass Between Two Lines in 3d Percolation

Luciano R. da Silva,*† Gerald Paul,* Shlomo Havlin,*‡ Don R. Baker,*§ and H. Eugene Stanley*
*Center for Polymer Studies and Dept. of Physics, Boston University, Boston, MA 02215 USA
†Departamento de Fisica, UFRN, 59072-970, Natal - RN Brazil
‡Department of Physics, Bar-Ilan University, Ramat-Gan, Israel
§Department of Earth and Planetary Sciences, McGill University
3450 rue University, Montrèal, QC H3A 2A7 Canada
(spbs.tex 26 December 2001 draft)

We consider the cluster and backbone mass distributions between two lines of arbitrary orientations and lengths in porous media in three dimensions, and model the porous media by bond percolation at the percolation threshold p_c. We observe that for many geometrical configurations the mass probability distribution presents power law behavior. We determine how the characteristic mass of the distribution scales with such geometrical parameters as the line length, w, the minimal distance between lines, r, and the angle between the lines, θ. The fractal dimensions of both the cluster and backbone mass are independent of w, r, and θ. The slope of the power law regime of the cluster mass is unaffected by changes in these three variables. However, the slope of the power law regime of the backbone mass distribution is dependent upon θ. The characteristic mass of the cluster also depends upon θ, but the characteristic backbone mass is only weakly affected by θ. We propose new scaling functions that reproduce the θ dependence of the characteristic mass found in the simulations.

I. INTRODUCTION

Since the 1950s, the percolation model has been applied to many disordered systems [1–4], and continues to be useful today. Here we use percolation theory to analyze the cluster and the backbone mass distributions of clusters that are connected in configurations of the type shown in Fig. 1, configurations in which the two lines are connected by occupied bonds. The *cluster mass* is the number of bonds that are connected to the two lines (Fig. 1a). The *backbone* of the cluster is the set of bonds that are connected to the two lines through independent paths (i.e., paths that have no common bond [5–8]). For configurations of two points, the distributions of various quantities have been studied [9–15]. Recently the distribution of the shortest paths between two lines has been studied for a three-dimensional cubic lattice [13], and here we calculate the mass and backbone distributions.

The motivation for this study is its relevance to techniques of oil recovery in oil fields [16]. A common technique used in oil recovery is the injection of fluid into the ground at one site in the field in order to force oil out of the ground at another site nearby (Fig. 1). It is common to inject the fluid along a portion of the length of the injection well and to collect the oil along a portion of the length of the production well (as opposed to injecting and collecting at single points on the wells). In our model, each line represents a well in the oil field. One line represents the injection well, and the other the production well. In many cases the oil reservoir is extremely heterogeneous, and the percolation model is appropriate. Separation of the rocks into two types—high permeability ("good rock") and low or zero permeability ("bad rock")—can be accomplished at the outset, with the good rock represented by occupied bonds and the bad rock represented by unoccupied bonds. The connected mass represents the total oil in the reservoir connected to the two wells, and the backbone mass the recoverable oil.

II. SIMULATIONS

We perform a numerical study of the system using Monte Carlo simulations. We specify two sets of points representing lines in a simple cubic lattice to be the wells and we grow the cluster from these two lines of seeds. If the growth of either cluster stops before the two clusters connect, we discard the realization. For realizations in which the two clusters connect, the simulation ends either when the cluster growth stops naturally, or when the cluster mass reaches some specified limit. To eliminate finite size effects, we use the techniques of Ref. [13] to simulate systems on lattices of large enough size that the clusters never reach the edge of the lattice. We perform the simulations at the percolation threshold, $p_c = 0.2488126$ [17]. The configurations are characterized by three parameters: length w, angle θ, and minimal distance r [see Fig. 1(a)]. For each configuration, we run at least 10^6 non-discarded realizations. We calculate the cluster and backbone mass for each of these realizations as exemplified in Fig. 1(b).

III. GENERAL OBSERVATIONS

In both the cluster mass and backbone mass distributions we expect to observe an initial cutoff due to the fact that these masses cannot be smaller than the distance r. In the backbone distributions, we expect to see a second cutoff due to the fact that the backbone mass cannot be greater than the cluster mass at which we stop the simulations. In addition, for both types of distributions we expect to observe a regime that exhibits power-law behavior. These general features of the distributions have been observed in the distributions for other quantities [9–13]. The quantities of interest are (i) the most-probable value of the distribution (the maximum), the scaling of which will be determined by the fractal dimensions of the quantities measured, and (ii) the slope of the power-law regime. For clusters grown from a single point, the slopes of the power law regimes of the cluster and backbone distributions are $\tau - 1$ and $\tau_B - 1$, where τ is the Fisher exponent and τ_B the corresponding exponent for the backbone. The fractal dimensions and power law regime slopes are related by [3,1,5]

$$\tau - 1 = \frac{d}{d_f} \tag{1}$$

$$\tau_B - 1 = \frac{d}{d_B}, \tag{2}$$

where d is the dimension of the system, and d_f and d_B are the fractal dimensions of the cluster and the backbone, respectively. For $d = 3$, estimates for these exponents are [18,19]

$$d_f = 2.524 \pm 0.008 \tag{3a}$$

$$d_B = 1.855 \pm 0.015 \tag{3b}$$

$$\tau - 1 = 1.189 \pm 0.004 \tag{3c}$$

$$\tau_B - 1 = 1.617 \pm 0.013. \tag{3d}$$

IV. CLUSTER MASS

A. Parallel Wells

In order to gain insight into the general behavior, we first study parallel wells ($\theta = 0$) see Fig. 2(a). We consider first the following limiting cases:

(i) $w \ll r$ — In this case we approximate the configuration by two points (see Fig. 2(b)). In Fig. 3(a) we show the mass probability distribution $P(m|r)$ for $w = 0$ and r = 1, 2, 4, 8, 16, 32 and 64. The distribution shows a maximum followed by a power-law regime with slope -1.18, consistent with Eq. (3c). We study also how the characteristic mass m^*, corresponding to peak of the distribution, scales with the distance r. The log-log plot of m^* vs r in Fig. 3b indicates that m^* scales with exponent $d_B \cong 2.6$ which is consistent with Eq. (3a).

(ii) $w \gg r$ — For this case [see Fig. 2(c)] we approximate the configurations by $r = 0$ (a single line). We perform the same analysis as before, and obtain similar results [see Fig. 4(a)], i.e., power law distribution for $P(m|w)$ with a slope ≈ -1.18 and fractal dimension ≈ 2.55 [Fig. 4(b)].

We now study cases intermediate to those studied in (i) and (ii). In Fig. 5a, we plot the distribution of cluster mass for configurations in which $r = 16$ and we vary w from 0 to 64. For small w, the distributions are essentially unchanged, but for $w \gg r$, the distributions scale with the exponent d_f (Fig. 5a and 5b).

We now develop a scaling form for the dependence of the characteristic mass m^* on r and L, the system size. Without loss of generality we can write

$$m^*(r, L) = \left[f\left(\frac{r}{w}\right) r \right]^{d_f}. \tag{4}$$

This form is consistent with the scaling of the cluster mass. That is, if

$$\begin{aligned} r' &\equiv \alpha r \\ w' &\equiv \alpha w, \end{aligned} \tag{5}$$

then

$$m^*(r', L') = \left[f\left(\frac{r'}{w'}\right) r' \right]^{d_f} = \left[f\left(\frac{r}{w}\right) \alpha r \right]^{d_f} = \alpha^{d_f} m^*(r, L). \tag{6}$$

We further assume that $m^*(r, L)$ can be written as

$$m^*(r, L) = \left[ar + g\left(\frac{r}{w}\right) w \right]^{d_f}, \tag{7}$$

since w and r become irrelevant variables for $r \gg w$ and $r \ll w$, respectively. Thus we expect

$$g\left(\frac{r}{w}\right) \to \begin{cases} 0 & r \gg w \\ \text{constant} & r \ll w \end{cases}. \tag{8}$$

B. Non-Parallel Wells

We now study non-parallel wells. The results for the mass probability distribution $P(m|\theta)$ are shown in Fig. 6(a). We find that the power law regime is consistent with a slope -1.18 independent of θ. We consider also the peak of these distributions, analyzing how m^* evolves with θ. Figure 6(b) shows the dependence of m^* versus θ. In this case we do not find a power distribution for the scaling behavior m^* versus θ. m^* increases rapidly for small values of θ, and for larger θ asymptotically approaches a limiting value at $\theta = \pi$.

We now suggest a functional form for the dependence of the characteristic mass m^* on θ. Without loss of generality we can write

$$m^*(\theta) = m^*(0)[f(\theta)]^{d_f}. \tag{9}$$

Since the configuration for $\theta = \pi$ is simply a single straight line twice the length of the single line for $\theta = 0$, we expect

$$m^*(\pi) = m^*(0) 2^{d_f}. \tag{10}$$

We then are motivated to write

$$m^*(\theta) = m^*(0)[1 + g(\theta)]^{d_f}, \tag{11}$$

where $g(\theta)$ is monotonic and

$$g(0) = 0$$

and

$$g(\pi) = 1.$$

A first guess at a functional form for $g(\theta)$ is some power of $\sin(\theta/2)$ but no power seems to fit the data of Fig. 6(b) well. A functional form that fits better is

$$h(\theta) = \sin\left[\frac{\pi}{2}\sin\left(\frac{\theta}{2}\right)\right]^{0.4}. \tag{12}$$

The final functional form for $m^*(\theta)$ is thus

$$m^*(\theta) = m^*(0)\left(1 + \sin\left[\frac{\pi}{2}\sin\left(\frac{\theta}{2}\right)\right]^{0.4}\right)^{d_f}, \tag{13}$$

where the exponent 0.4 is obtained by the power law fit in Fig. 7(a). We note that there is no *a priori* justification for this form; it simply satisfies the appropriate boundary conditions and fits the simulation results reasonably well, as shown in Fig. 7(b).

V. BACKBONE MASS

We proceed to analyze the scaling of the backbone mass distributions as we did for the cluster mass.

A. Parallel Wells

(i) $w \ll r$ — We present in Fig. 8(a) the backbone probability distribution $P(m_B|r)$. As seen in Fig. 8(a) and (b), the power law regimes of these plots are consistent with Eq. (3d), and the distributions scale with an exponent consistent with d_B. Similar results have been found previously [12] but are shown here for completeness.

(ii) $w \gg r$ — We show in Fig. 9(a) the backbone probability distribution $P(m_B|w)$ for this case. Again, the power law regimes of these plots are consistent with Eq. (3d) and the distributions scale asymptotically with an exponent consistent with d_B [Fig. 9(b)] although there are large corrections-to-scaling as seen in the small w behavior of Fig. 9(b).

Figures 9(a) and 9(b) are also indicative of the behavior of cases intermediate to the limiting cases of (i) and (ii) above. For $w \ll r$, changing w will have essentially no effect on the distributions; for $w \gg r$, the distributions will scale with d_B as w is changed.

B. Non-Parallel Wells

We show the results for the backbone probability distribution $P(m_B|\theta)$ in Fig. 10(a) for various values of θ. In contrast to the distributions of cluster mass, the distributions of backbone mass exhibit power-law regimes, the exponents of which depend on θ while the characteristic mass m^*, is essentially constant as a function of θ. Thus an appropriate functional form for $P(m_B|\theta)$ is

$$P(m_B|\theta) \sim \left(\frac{m_B}{r^{d_B}}\right)^{g_B(\theta)} f_1\left(\frac{m_B}{r^{d_B}}\right) f_2\left(\frac{m_B}{L^{d_B}}\right), \tag{14}$$

where f_1 and f_2 are cutoff functions. The first cutoff function, f_1, reflects the fact that the backbone mass must always be at least equal to the distance r between the two points; the second cutoff function, f_2, reflects the fact that the backbone mass is bounded because of the finite size, L, of the system. Similar behavior has been observed for the distributions of shortest paths between two lines [13].

In order to determine the varying slope more accurately we perform simulations for various θ for $r = 1$, which results in the largest power-law regime. The results of these simulations are shown in Fig. 10(b). In Fig. 10(c) we plot the power-law regime exponent, g_B vs θ. For $\theta = 0$, the configuration is that of parallel lines, and the exponent is τ_B. For $\theta = \pi$, the exponent decreases to a value of about 0.84. The marked difference in these two exponents is shown clearly in Fig. 11, in which we plot for fixed $r = 1$, $\theta = 180°$, $P(m_B|r)$ for various values of w. The larger the value of w, the later a crossover occurs from behavior reflecting a configuration of 2 lines with $\theta = 180°$ to a configuration effectively of 2 points, with power-law-regime exponent $\tau_B - 1$.

VI. DISCUSSION

We have analyzed the distributions of cluster mass and backbone mass for various configurations of 2-line 3d percolation clusters. The behavior of the cluster mass distributions is not remarkable. On the other hand, we have found that the exponent of the power-law-regime for the backbone mass distributions is dependent on the angle θ between the lines. It remains to develop a theory which can predict the specific dependence of this exponent on θ.

Acknowledgements

We thank L. Braunstein and S. V. Buldyrev for helpful discussions, and British Petroleum, CPNq, and the National Science Foundation for support.

---

[1] A. Bunde and S. Havlin, eds., *Fractal and Disordered Systems, Second Edition* (Springer-Verlag, Berlin, 1996), and references therein.

[2] D. Ben-Avraham and S. Havlin, *Diffusion and Reactions in Fractals and Disordered Systems* (Cambridge University Press, Cambridge, 2000).

[3] D. Stauffer and A. Aharony, *Introduction to Percolation Theory* (Taylor and Francis, London, 1992).

[4] M. Sahimi, *Applications of Percolation Theory* (Taylor and Francis, London, 1992).

[5] H. J. Herrmann and H. E. Stanley, Phys. Rev. Lett. **53**, 1121 (1984).

[6] H. E. Stanley, J. Phys. A: Math. Gen. **10**, L211 (1977).

[7] A. Coniglio, Phys. Rev. Lett. **46**, 250 (1981).

[8] S. Havlin and Ben-Avrahan, Adv. Phys. **36**, 695 (1987).

[9] N. V. Dokholyan, Y. Lee, S. V. Buldyrev, S. Havlin, P. R. King and H. E. Stanley, J. Stat. Phys. **93**, 603 (1998).

[10] Y. Lee, J. S. Andrade, Jr., S. V. Buldyrev, S. Havlin, P. R. King, G. Paul, and H. E. Stanley, Phys. Rev. E **60**, 3425 (1999).

[11] J. S. Andrade Jr., S. V. Buldyrev, N. Dokholyan, P. R. King, Y. Lee, S. Havlin, and H. E. Stanley, Phys. Rev. E **62**, 8270 (2000).

[12] M. Barthélémy, S. V. Buldyrev, S. Havlin, and H. E. Stanley, "Scaling for the Critical Percolation Backbone," Phys. Rev. E **60**, R1123 (1999).

[13] G. Paul, S. Havlin, and H. E. Stanley, "Fractal Behavior of the Shortest Path Between Two Lines in Percolation Systems" (preprint).

[14] P. Grassberger, J. Phys. A: Math. Gen. **32**, 6233 (1999).

[15] R. M. Ziff, J. Phys. A **32**, L457 (1999).

[16] P. R. King, in *North Sea Oil and Gas Reservoirs II*, edited by A. T. Buller et al. (Graham and Trotman, London, 1990).

[17] C. D. Lorenz and R. M. Ziff, Phys. Rev. E **57**, 230 (1998).

[18] R. M. Ziff and G. Stell, preprint; P. N. Strenski, R. M. Bradley, J. M. Debierre, Phys. Rev. Lett. **66**, 133 (1991).

[19] M. D. Rintoul and H. Nakanishi, J. Phys. A **27**, 5445 (1994).

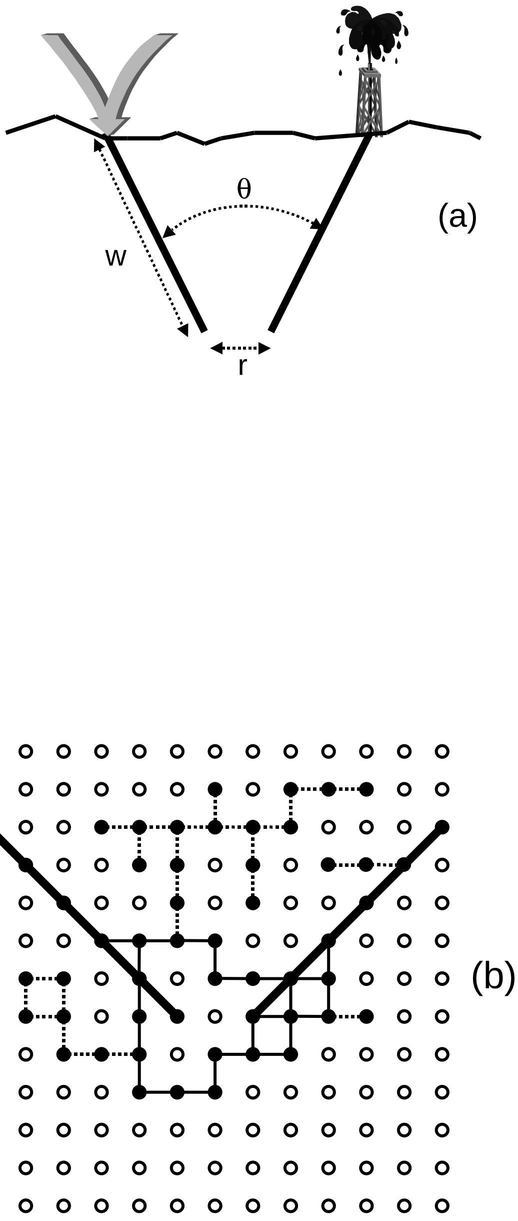

FIG. 1. (a) Illustration of well geometry. (b) Examples of a percolation cluster with two line wells with parameters $r = 2$, $\theta = 90^\circ$, and $w = \sqrt{50}$. The filled sites are members of the percolation cluster, which has a mass of 52. Solid lines form the backbone, which has a mass of 28.

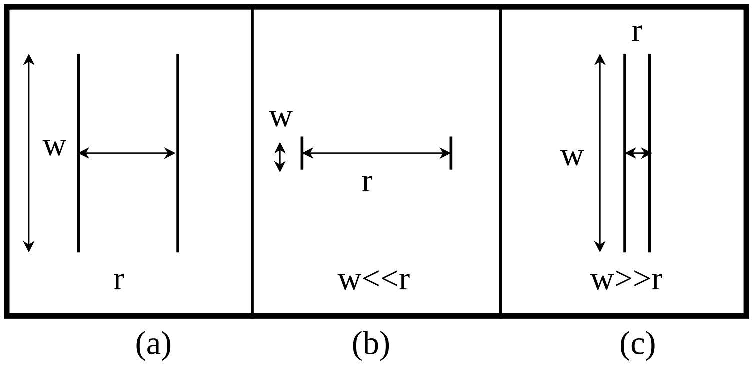

FIG. 2. Parallel well examples. (a) general case (b) $w \ll r$ (c) $w \gg r$.

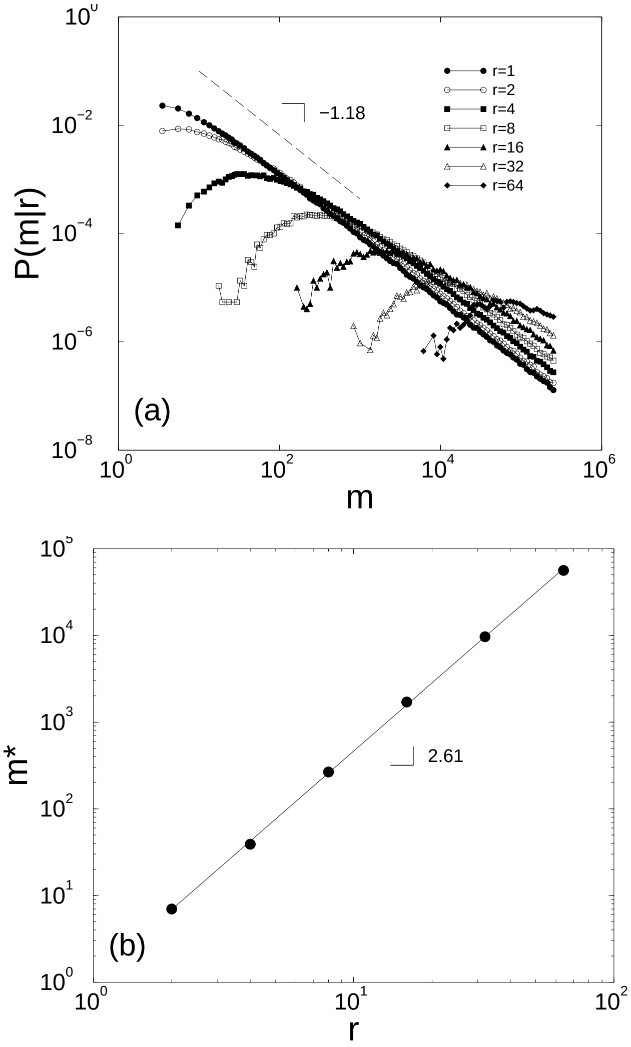

FIG. 3. (a) Cluster mass distribution $P(m|r)$, for the percolation cluster for the two points case ($w = 0$), for several values of r ($r = 1, 2, 4, 8, 16, 32, 64$). The line of slope -1.18 denotes the theoretical expectation. (b) Scaling behavior of m^*, the most probable mass, as a function of r. The fitted slope of 2.61 is consistent with the fractal dimension $d_f = 2.54$

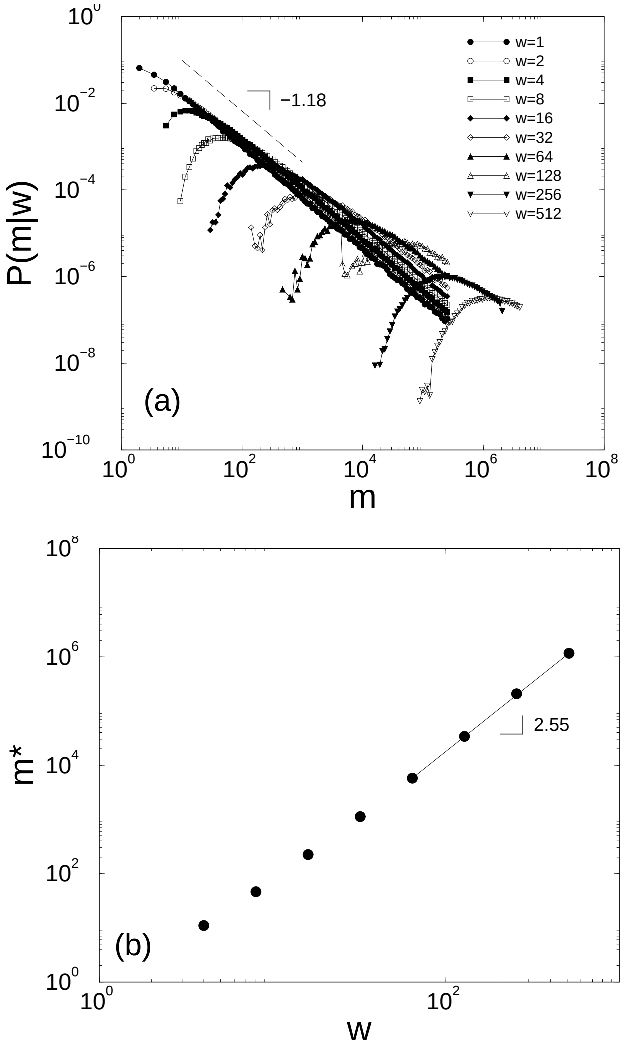

FIG. 4. (a) Cluster mass distribution $P(m|w)$ for $(r = 0)$ for several values of w $(w = 1, 2, 4, 8, 16, 32, 64, 128, 256, 512)$. (b) Scaling behavior of m^* as a function of w.

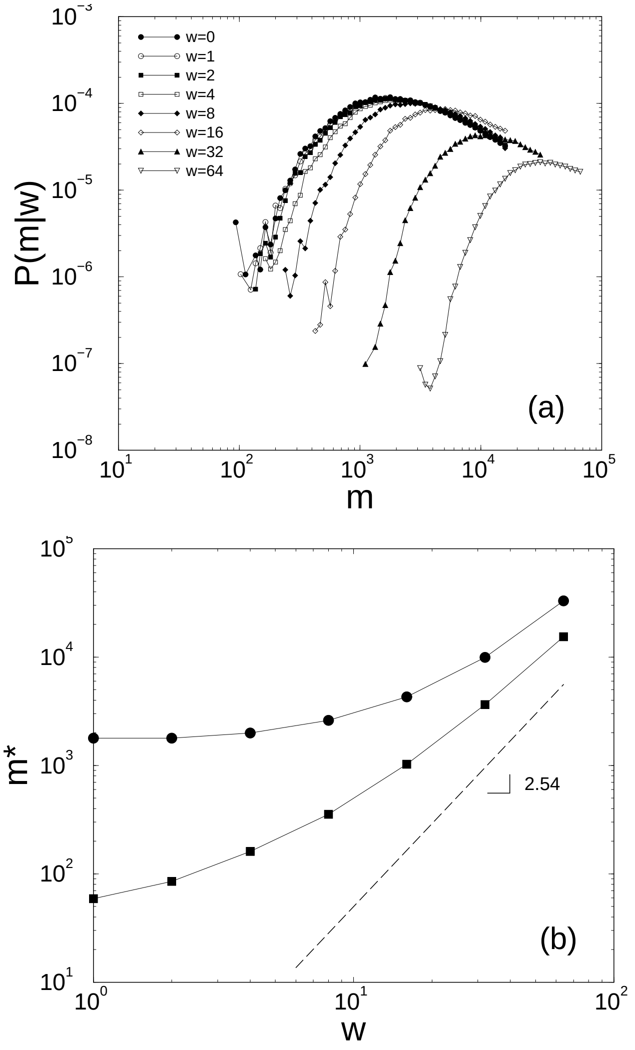

FIG. 5. (a) Mass distribution $P(m|w)$ for two parallel wells with $r = 16$ and $w = 0, 1, 2, 4, 8, 16, 32, 64$. (b) Scaling behavior of m^* versus w for $r = 4$ (circles) and for $r = 16$ (squares).

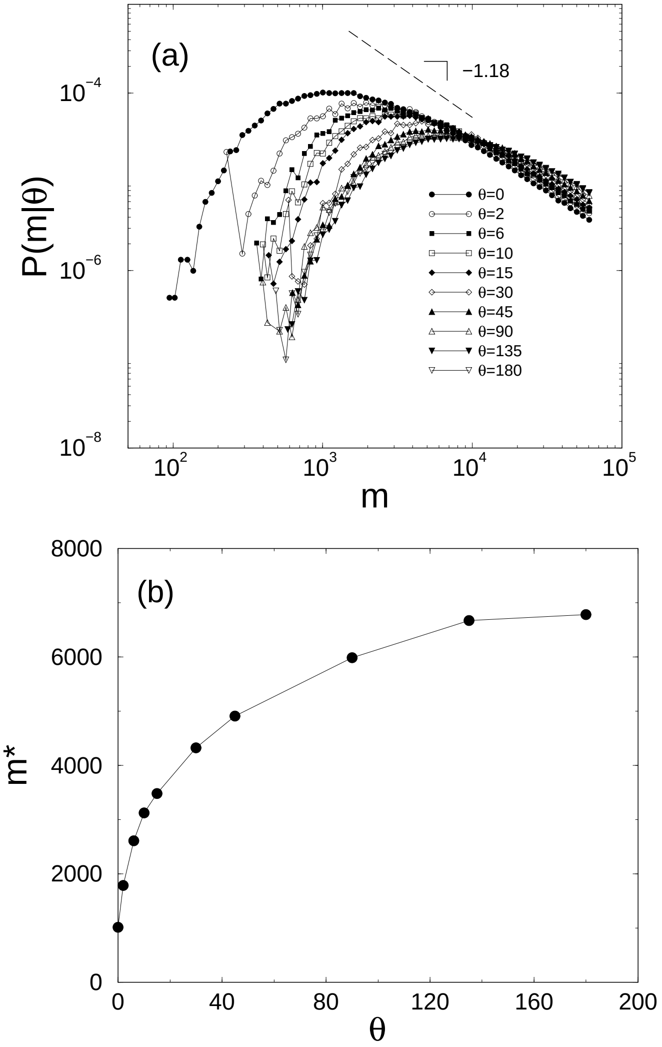

FIG. 6. (a) Mass distribution $P(m|\theta)$ for $r = 0$ and $w = 32$ for the percolation cluster to the general non parallel wells for several values of the angle θ. (b) Corresponding scaling behavior of m^* versus θ.

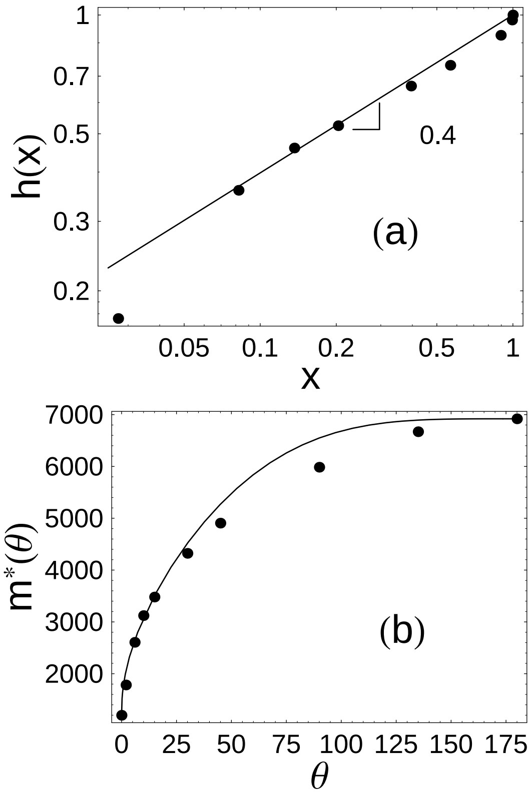

FIG. 7. (a) Determination of exponent in Eq. (12), where $x \equiv \sin[(\pi/2)\sin(\theta/2)]$. (b) Comparison of functional form $m(\theta)$ (solid line) versus observed data.

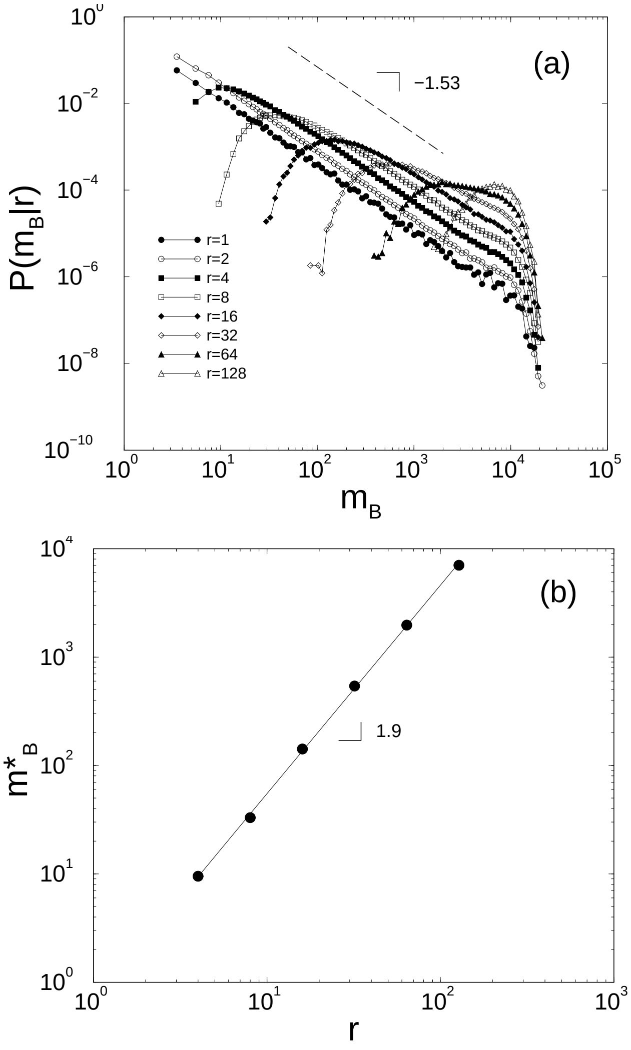

FIG. 8. (a) Backbone mass distribution $P(m_B|r)$ for the percolation cluster for two points and $r = 1, 2, 4, 8, 16, 32, 64, 128$ (b) Scaling behavior of m_B^* versus r.

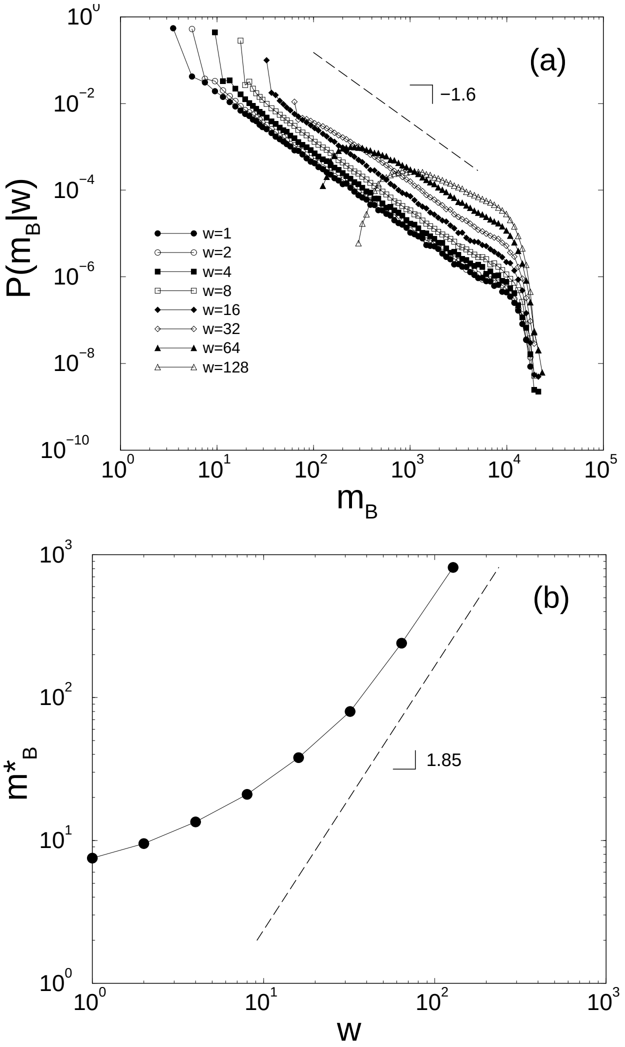

FIG. 9. (a) Backbone mass distribution $P(m_B|w)$ for parallel wells for $r = 1$ and $w = 1, 2, 4, 8, 16, 32, 64, 128$. (b) The corresponding scaling behavior of m^*_B versus w.

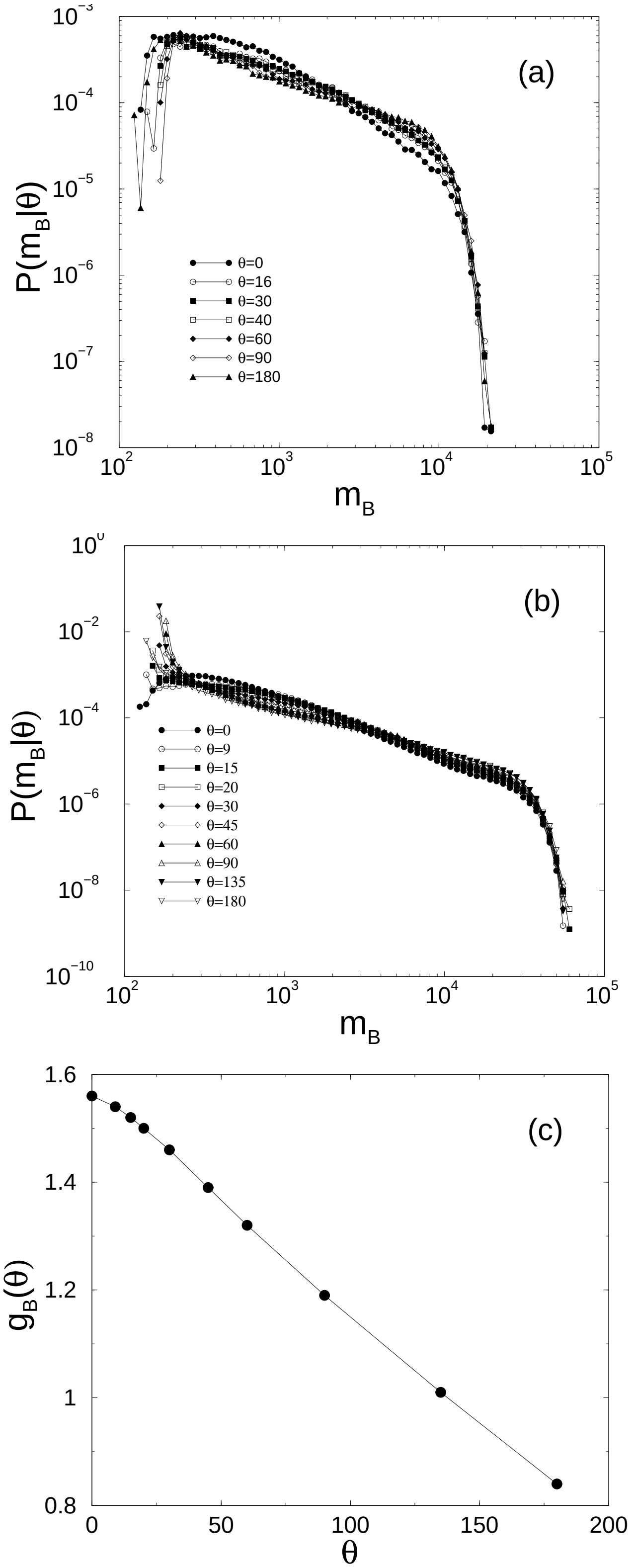

FIG. 10. (a) Backbone mass distribution $P(m_B|\theta)$ for non-parallel wells with $r = 8$, $w = 64$, and several values of θ. The cutoff of cluster growth is at a cluster mass of 2^{18}. (b) Backbone mass distribution $P(m_B|\theta)$ for the case of nonparallel wells with $r = 1$, $w = 64$ for various θ. The cutoff of cluster growth is at a cluster mass of 2^{20}. (c) Power law exponent $g_B(\theta)$, defined in Eq. (14), for the corresponding backbone mass distribution presented in (b).

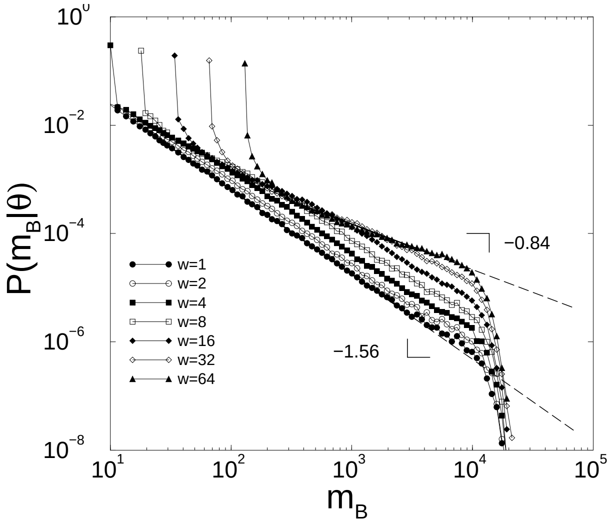

FIG. 11. Backbone mass distribution $P(m_B|w)$ for the non parallel wells for fixed θ $(= 180^\circ)$ and several values of w. The larger the value of w, the later a crossover occurs from behavior reflecting a configuration of 2 lines with $\theta = 180^\circ$ to a configuration effectively of 2 points, with power-law-regime exponent $\tau_B - 1$.